Kalman-Filter Based Hybridization of Classic and Cold Atom Interferometry Accelerometers for Future Satellite Gravity Missions

Alireza HosseiniArani, Benjamin Tennstedt, Manuel Schilling, Annike Knabe, Hu Wu, Steffen Schön, and Jürgen Müller

Abstract

Proof-of-principle demonstrations have been made for cold atom interferometer (CAI) sensors. Using CAI-based accelerometers in the next generation of satellite gravimetry missions can provide long-term stability and precise measurements of the non-gravitational forces acting on the satellites. This would allow a better understanding of climate change processes and geophysical phenomena which require long-term monitoring of mass variations with sufficient spatial and temporal resolution. The proposed accuracy and long-term stability of CAI-based accelerometers appear promising, while there are some major drawbacks in the long dead times and the comparatively small dynamic range of the sensors. One interesting way to handle these limitations is to use a hybridization with a conventional navigation sensor. This study discusses one possible solution to employ measurements of a CAI accelerometer together with a conventional Inertial Measurement Unit (IMU) using a Kalman filter framework.

A hybrid navigation solution of these two sensors for applications on ground has already been demonstrated in simulations. Here, we adapt this method to a space-based GRACE-like gravimetry mission. A simulation is performed, where the sensitivity of the CAI accelerometer is estimated based on state-of-the-art ground sensors and further published space scenarios. Our results show that the Kalman filter framework can be used to combine the measurements of conventional inertial measurement units with the CAI accelerometers measurements in a way to benefit from the high accuracy of the conventional IMU measurements in higher frequencies together with the high stability of CAI measurements in lower frequencies. We will discuss the challenges, potential solutions, and the possible performance limits of the proposed hybrid accelerometry scenario.

Keywords

Atom interferometry · Hybrid accelerometer · Quantum sensor · Satellite gravimetry

A. HosseiniArani (✉)
Leibniz University Hannover, Institute of Geodesy, Hannover, Germany

German Aerospace Center, Institute for Satellite Geodesy and Inertial Sensing, Hannover, Germany
e-mail: hosseiniarani@ife.uni-hannover.de

B. Tennstedt · A. Knabe · S. Schön · J. Müller
Leibniz University Hannover, Institute of Geodesy, Hannover, Germany

M. Schilling
German Aerospace Center, Institute for Satellite Geodesy and Inertial Sensing, Hannover, Germany

International Association of Geodesy Symposia,
https://doi.org/10.1007/1345_2022_172,

1 Introduction

The satellite gravimetry missions GRACE and GRACE-FO have enabled the monitoring of the global time variable gravity field. The results contributed to quantifying mass changes related to climate change (Tapley et al. 2019) and new insights into processes of the Earth's interior (Mandea et al. 2020). The gravity field solutions are limited in the very low degrees at C_{20} and, for times with only one operational accelerometer on two satellites, even at C_{30} (Loomis et al. 2020). These coefficients are typically replaced with satellite laser ranging solutions. The spatial resolution is limited at a few hundred kilometers for the typical monthly gravity field solutions. For future missions a resolution at the order of 100 km or below is needed to address the requirements of the scientific community (Pail et al. 2015). This would allow, amongst others, to monitor the mass balance of smaller glaciers or contribute to the water management as well as drought or flood predictions on a regional scale.

The GRACE-FO mission added a laser ranging interferometer (LRI) as a major innovation compared to the K-band ranging system (KBR) on the GRACE mission. Currently the LRI is a technical demonstrator for inter-satellite ranging and GRACE-FO still employs KBR as the main instrument. Future missions will probably rely on a LRI system (see e.g. Haagmans et al. 2020) because the current LRI performance already exceeds the mission requirements of $80\,\mathrm{nm}/\sqrt{\mathrm{Hz}}$ (Abich et al. 2019) and the GRACE KBR noise of $1\,\mu\mathrm{m}/\sqrt{\mathrm{Hz}}$. The performance of the electrostatic accelerometer (ACC) for GRACE-FO, however, has not changed significantly from the GRACE mission (Christophe et al. 2015).

Figure 1 shows the ACC and ranging system error models of GRACE and GRACE-FO as amplitude spectral densities in range accelerations. The potential improvement of the gravity field solutions is in the frequency range above 10^{-3} Hz. One of the main deficiencies of GRACE gravity field solutions, the so called striping effect, is not improved in GRACE-FO solutions. This effect, which manifests itself as low frequency stripes in the spatial domain, is caused by the predominantly North–South direction of the observations, unmodelled temporal variations of atmosphere and ocean, but also a drift of the ACC in frequencies below 10^{-3} Hz. The stripes are typically reduced by signal processing, e.g. a 300 km Gaussian filter, which, however, also affects the gravity signal.

The development of electrostatic ACC for future missions (e.g. Christophe et al. 2018) shows an improvement in instrumental noise by more than one order of magnitude for frequencies above 10^{-3} Hz while keeping an approximately $1/\sqrt{f}$ low frequency drift. Cold Atom Interferometry (CAI; see Sect. 2) is one potential technology to overcome the limitation of the electrostatic ACCs in lower frequencies. Additionally, the CAI measurement enables the calibration of the electrostatic accelerometer by a second bias and drift free in-situ measurement of the non gravitational accelerations. Currently, this type of calibration step uses modelled non-gravitational accelerations (see e.g. Klinger and Mayer-Gürr 2016; Wöske et al. 2019).

The proposed accuracy and long-term stability of CAI-based accelerometers appear promising, while there are some major drawbacks in the long dead times and the comparatively small dynamic range of the sensor. One promising way to handle the drawbacks of atom interferometry is to use it in hybrid combination together with conventional navigation sensors. The CAI measurement then has to be combined with the electrostatic ACC, for which we present a Kalman filter based approach (Sect. 3) to create a hybrid one-axis accelerometer (Sect. 4) oriented in the along-track direction.

2 Orbit and Accelerometer Modelling

2.1 Cold Atom Interferometer Accelerometry

Cold Atom Interferometry utilises atoms as test masses in an interferometer realised by a sequence of specific laser pulses. A light pulse atom interferometer can be implemented in different ways. See Abend et al. (2020) for an overview. Only a brief introduction based on Kasevich and Chu (1991) is given here. The atom interferometer consists of three laser pulses acting as either beam splitter or mirror. The frequencies of two parallel counter-propagating lasers beams are chosen to be in resonance with a two-photon Raman transition. The first light pulse creates a beam splitter, putting about 50 % of the atoms in a superposition of the initial state with an excited state (having absorbed energy and momentum of two photons). After a time interval T a second light pulse initiates a transition of all atoms from excited back to initial state or vice versa. After a second time interval T a second beam splitter closes the interferometer. The leading order atom interferometer phase $\Delta\Phi$ is described by

$$\Delta\Phi = (\mathbf{k}_{\mathrm{eff}} \cdot \mathbf{a} - \alpha)T^2 + \Phi_L \tag{1}$$

with the acceleration $\mathbf{a}$ acting on the atoms and the effective optical wave vector of the laser light $\mathbf{k}_{\mathrm{eff}}$, which describes the photon momentum exchange.[1] The Raman laser phase Φ_L is added to the last light pulse to operate the interfer-

[1] The momentum transferred is $\hbar\mathbf{k}_{\mathrm{eff}}$ where $\hbar$ is the reduced Planck constant.

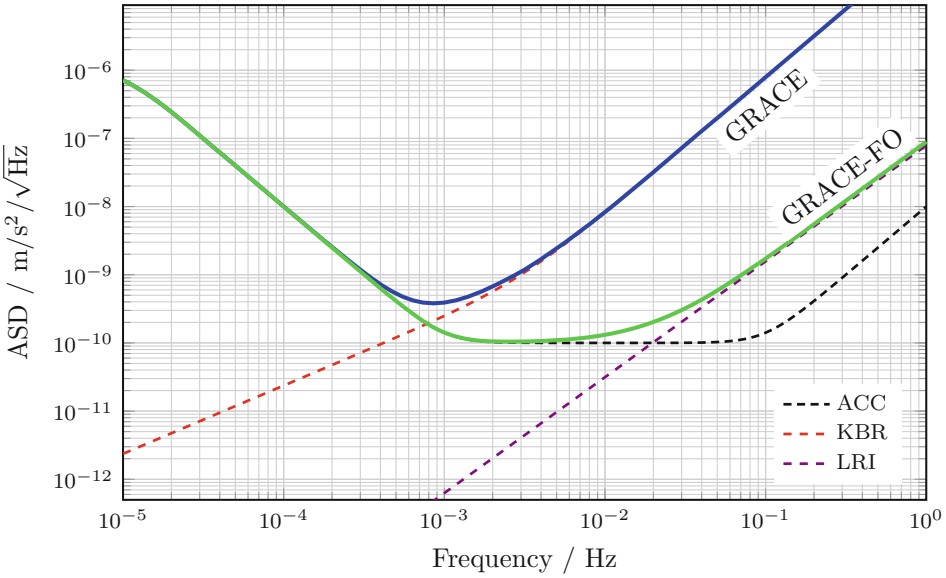

Fig. 1 Amplitude spectral densities in range accelerations in the along-track direction of dominant noise sources for GRACE(-FO) satellite missions with electrostatic accelerometer (ACC; Flury et al. 2008; Christophe et al. 2015) and microwave- or laser-ranging system (KBR,LRI; Thomas 1999; Abich et al. 2019). ACC performance includes an estimate for temperature dependent bias variations in low frequencies (Christophe et al. 2018)

ometer, e.g., mid-fringe (cf. Sect. 3.2). The linear frequency ramp α is added to compensate for the acceleration of the atoms. The acceleration in direction of $\mathbf{k}_{\text{eff}}$ is canceled out if $\alpha = |\mathbf{k}_{\text{eff}} \cdot \mathbf{a}|$. This way, all measurements of a CAI can be traced back to (laser) frequencies. More specifically, $\Delta\Phi$ measures the projection of the acceleration $\mathbf{a}$ along $\mathbf{k}_{\text{eff}}$, e.g. in terrestrial applications $\mathbf{k}_{\text{eff}}$ is aligned in parallel to $\mathbf{g}$ to create a gravimeter. In a satellite setting, $\mathbf{a}$ are the non-gravitational accelerations acting on the satellite. Assuming the CAI is in the center of mass and $\mathbf{k}_{\text{eff}}$ is aligned in the along-track direction, $\Delta\Phi$ would be a measure of the non-gravitational accelerations in the along-track direction.

According to Eq. (1) the sensitivity of the CAI can be increased by either applying methods with a higher photon momentum transfer (e.g. multiphoton Bragg diffraction) or increasing the pulse separation time T. For terrestrial applications T is limited by the length of the free fall distance of the atoms, e.g. up to 300 ms for a transportable (Freier et al. 2016) and 1.2 s for a stationary instrument (Schilling et al. 2020). As atoms and satellites in space are in free fall, these restrictions do not apply and longer times T are possible. Limiting factors are, for example, the thermal expansion of the atomic cloud.

The technical realisation of the CAI is of lesser importance at this stage. Considering the intended duration of a single interferometer sequence, using Bose-Einstein Condensates might also be the preferred choice (Becker et al. 2018). In this study, individual measurements of the CAI-ACC have a certain duration and its time series have certain spectral properties while the measurements are also affected by external effects like rotations.

2.2 In-Orbit Simulation of Electrostatic and CAI Accelerometers

In this study we consider a GRACE-like satellite pair in a circular polar orbit around the Earth with an altitude of 480 km. The simulation is implemented in the MATLAB/Simulink based eXtended High Performance satellite dynamics Simulator (XHPS; Wöske et al. 2019) developed by ZARM/DLR. XHPS calculates the orbits of a GRACE-FO mission scenario under consideration of the Earth's gravity field 'EGM2008' (up to d/o 90), non-gravitational forces (atmospheric drag, solar radiation pressure, Earth albedo and thermal radiation pressure) and the GRACE satellite geometry. To consider the effect of non-gravitational forces on the spacecraft, we use a detailed surface model of the satellite body included in XHPS.

The IMU measures the linear accelerations and angular rates acting on the satellite. In this study, we consider a simplified case, where we assume to have a perfect knowledge of the angular velocities and therefore, only the measurements of linear accelerations by an electrostatic accelerometer (E-ACC) are considered as the measurements of conventional IMU.

The E-ACC measures the sum of non-gravitational accelerations acting on the satellite in three orthogonal directions (along-track, cross-track and radial). The sensor model of an E-ACC, based on the GRACE ACC sensitive axis with a noise level of $10^{-10}\,\text{m/s}^2/\sqrt{\text{Hz}}$ in frequencies above 10^{-3} Hz, is implemented in XHPS. The sampling rate of the E-ACC is 10 Hz.

Later during this study, we also use a more accurate model of E-ACC with a noise level of $10^{-11}\,\text{m/s}^2/\sqrt{\text{Hz}}$ in

frequencies above 10^{-3} Hz and test the performance of its hybridization with the CAI-ACC model.

The functionality of the algorithm also depends on the accelerometer noise in timescales of the CAI measurement duration. Although better performing E-ACC have already been flown in space (e.g. GOCE; Marque et al. 2010) or are published as recent developments (Christophe et al. 2018), the GRACE-FO type accelerometer was chosen to later compare with GRACE-FO gravity field solutions. This scenario is also a worst case scenario, i.e. if our method works successfully for this accelerometer, an accelerometer with a lower noise is not a priority to enable a hybrid accelerometer. A conventional E-ACC usually has its best performance in higher frequencies, while at lower frequencies the measurements suffer from a large noise. The low frequency noise shows its impact on the measured accelerations as a bias (see Fig. 4). The accelerometer measurements therefore can be written as:

$$A_{ACC} = B + S \cdot A_{non\text{-}grav.} + N \tag{2}$$

where B is the accelerometer bias, S is the accelerometer scaling factor and N stands for the random noise. In this study, we ignore the scaling factor and focus on the determination of the E-ACC bias.

For the CAI-ACC a white noise at the level of 10^{-10} m/s^2/$\sqrt{\text{Hz}}$ is assumed. The assumption is based on the results of terrestrial applications (e.g. Freier et al. 2016) and the fact that the CAI measurement is directly related to the frequency stability of the laser system (see also Eq. (1) and Abich et al. 2019; Sanjuan et al. 2021). As shown by Abrykosov et al. (2019), a CAI-ACC with a higher noise level will not improve the gravity field solution. Therefore, it is also unlikely that a gravity field mission will be launched with a CAI-ACC performing not at least at this level (Alonso et al. 2022).

The signal of the CAI accelerometer is modelled based on Eq. (1). However, because of the change of the non-gravitational acceleration during the CAI interrogation time, we integrate this equation by considering the sensitivity function of CAI as described in Knabe et al. (2022).

For the noise modelling, we use a band-limited white noise in the frequency range of 10^{-5} Hz to 10^{-1} Hz from which we produce a noise time series. Then, we add this noise to the acceleration signal and calculate the measured phase of the cold atom interferometry accelerometer.

3 Extended Kalman Filter

The benefit of the hybridization of cold atom and electrostatic accelerometers for gravity field missions under certain circumstances has already been shown (e.g. Abrykosov et al. 2019). These studies typically generate noise-only time series for the two accelerometers and combine them, e.g., by filtering. The hybrid accelerometer noise, converted to ranging accelerations, is then added to the ranging observations prior to gravity field recovery. Our method aims at combining the (noisy) measurements of the two accelerometers while simultaneously using the measurements of the electrostatic accelerometer to solve phase ambiguities of the cold atom interferometer. The method introduced here can potentially be used in real time for data generated by future hybrid sensors and has already been demonstrated by experiment for application in inertial navigation (Weddig et al. 2021).

The measurements of the CAI and the electrostatic ACC have different sampling rates, e.g. 0.1 Hz and 10 Hz, which have to be combined to create a hybrid accelerometer. In this study, we adapt an extended Kalman filter (EKF) based approach used for inertial navigation (Tennstedt and Schön 2021). This filter system uses the E-ACC data as input to the dynamic model in order to predict the phase shift and the expected observation of the atom interferometer, effectively solving the fringe ambiguity. The CAI data is then used as actual observation in return to estimate the bias of the E-ACC. The equations are stated for a system oriented in the along-track direction. This can be realized by a single CAI sensor with its sensitive axis oriented along the respective spatial axis of the body-frame of the vehicle.

The functionality of the algorithm depends on the amplitude of the input signal (non-gravitational accelerations) as well as the change in a given time interval and these are largest in the along-track direction for our scenario. The amplitude and change of signal for the cross-track and radial axis are smaller and require less accuracy from the electrostatic accelerometer to solve the phase ambiguity of a single measurement.

3.1 Dynamic System and Phase Prediction

The measurement of CAI and IMU is combined in the body-frame (b-frame), which is aligned with the CAI sensor. In order to predict the phase shift which is based on the position of the atoms in the laser field during the interrogation pulses, cf. Tennstedt and Schön (2021) and Antoine and Borde (2003), the motion equations of the atoms in the body-frame are utilized. The state vector reads

$$\mathbf{x} = [q^b, v^b, b_a]^T, \tag{3}$$

with v^b as atom velocity and q^b as atom position in the along-track direction in the body-frame affected by the accelerations and acceleration bias b_a of the electrostatic IMU.

The evolution of the kinematic state can be described by the following system of ordinary differential equations (ODE).

$$\dot{q}^b = v^b, \tag{4}$$

$$\dot{v}^b = f^b + b_a, \tag{5}$$

$$\dot{b_a} = 0, \tag{6}$$

where f^b are specific forces affecting the system, i.e. non-gravitational accelerations. It is assumed that the platform is stabilized and thus no Coriolis term due to the rotation occurs.

For the prediction step of the filter, this system is numerically solved by trapezoid integration. The predicted phase shift of the interferometer is given by (Tennstedt and Schön 2021):

$$\Phi_{pred} = k_{\text{eff}} \left(q^b(T_f) - 2q^b(\frac{1}{2}T_f) \right), \tag{7}$$

where the total filter step time T_f equals twice the interrogation time $T_f = 2T$. The two atom positions at T and $2T$ are gained from the numerical integration.

For the covariance propagation, the transition matrix $\mathbf{F}_k$ is needed. The systems solution after discretisation yields:

$$\mathbf{x}_{k+1} = \mathbf{F}_k \mathbf{x}_k + \mathbf{B}_k \mathbf{u}_k + \mathbf{w}_k. \tag{8}$$

The homogeneous part of the solution is characterized by the wanted transition matrix $\mathbf{F}_k$:

$$\mathbf{F}_k = \begin{pmatrix} 1 & \Delta t & 0 \\ 0 & 1 & \Delta t \\ 0 & 0 & 1 \end{pmatrix}, \tag{9}$$

where Δt is the filter time constant.

The particular solution with the input matrix $\mathbf{B}_k = [\frac{1}{2}\Delta t^2, \Delta t, 1]^T$ denotes any perturbations that affect the system, here mainly resembled by accelerations $\mathbf{u}_k = f^b$, as well as another additive noise component $\mathbf{w}_k$ to allow the adaption of the filter.

The system noise $\mathbf{Q}_k$ can be approximated:

$$\mathbf{Q}_k = \left(\mathbf{B}_k E[\mathbf{u}_k \mathbf{u}_k^T] \mathbf{B}_k^T + E[\mathbf{w}_k \mathbf{w}_k^T] \right) \Delta t. \tag{10}$$

The formal variance $E[\mathbf{u}_k \mathbf{u}_k^T]$ is used to include the E-ACC data uncertainty.

3.2 CAI Observation Equation

The CAI observation equation is based on the transition probability p that follows the sinusoidal fringe pattern:

$$p = A \cos(\Phi_L + \Phi_{pred} + \delta\Phi) + p_0. \tag{11}$$

The fringe amplitude A and zero offset p_0 are regarded as known constants over the time of the experiments. The laser phase Φ_L is assumed to be regulated by the controller so that the sum of $\Phi_L + \Phi_{pred}$ is always at the operating point $\pi/2$ (*mid-fringe*).

The error phase shift $\delta\Phi$ is the part that results from any errors of the accelerations measured by the conventional IMU, here biases. It couples the observation equation with the state parameters.

In order to enable a connection between this phase shift and the system model, Eq. (5) is utilized again. This time the equation is solved analytically under the assumption of a time-constant system during the measuring interval, making it easier to derive the matrix $\mathbf{H}$.

Since the filter is only active during the measurement cycle of the CAI, T_f essentially equals the filter time constant Δt that was introduced before.

The integrated acceleration bias leads to the following velocity increment:

$$\delta v = b_a T_f. \tag{12}$$

The equation for $\delta\Phi$ is then

$$\delta\Phi = \frac{1}{4} k_{\text{eff}} b_a T_f^2, \tag{13}$$

which is similar to the more familiar expression $\delta\Phi = k_{\text{eff}} a T^2$ from the first section. All discussed values plugged into Eq. (11) result in:

$$p = A \cos\left(\frac{\pi}{2} + \frac{1}{4} k_{\text{eff}} b_a T_f^2 \right) + p_0. \tag{14}$$

The final observation matrix $\mathbf{H} = \frac{\partial p}{\partial \mathbf{x}}$ reads:

$$\mathbf{H}^T = \begin{pmatrix} 0 \\ 0 \\ -\frac{1}{4} A \cdot k_{\text{eff}} T_f^2 \end{pmatrix}. \tag{15}$$

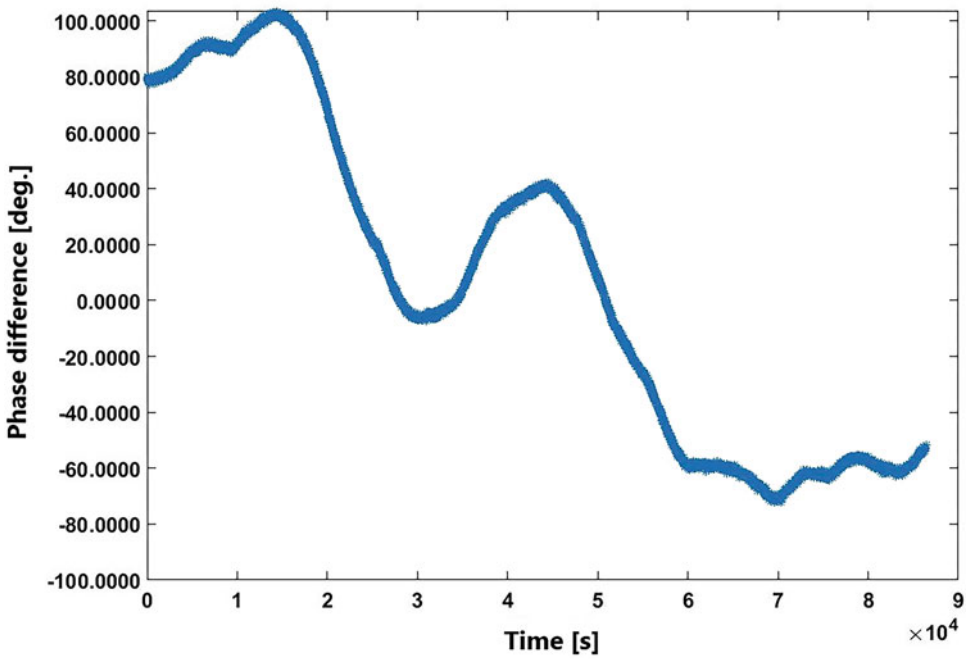

Fig. 2 The difference between the true CAI phase and the determined phase based on the E-ACC measurements in one day of the mission

Note that the constant system assumption is only necessary for the calculation of the measurement sensitivities in matrix **H**. The calculation of the innovation follows the original non-linear equations described before.

The observation uncertainty of the atom interferometer measurement is expressed in $R = \sigma_p^2$.

4 Results and Discussion

4.1 Solving for the Phase Ambiguity

The CAI sensor has a phase ambiguity which has to be solved for. Our approach here is to use the phase shift equivalent to the acceleration measured by E-ACC to determine the target part of the cosine interval. This only works if the bias and the integrated noise of the IMU in the respective measurement cycle is smaller than half of the cosine flank $\pi/2$.

In the case that the phase difference between the CAI and the predicted phase is higher than $\pi/2$, but lower than π, the filter will not be able to directly estimate the phase ambiguity. However, it will likely converge to the right direction and in the next iteration there is a good chance that the phase difference is further reduced. Therefore, after a few iterations, the CAI phase ambiguity will be estimated correctly.

Monte Carlo simulations of in-flight CAI-ACC and E-ACC are performed to study the phase differences and to verify whether or not this approach can be used for the case of satellite gravimetry. Those simulations show that in most of the cases (>95 %) the phase difference $\phi_{IMU} - \phi_{CAI}$ stays below the limit of π (see Fig. 2). The assumptions here are the satellite altitude of 480 km, the CAI interferometer duration of 10 s and assumed E-ACC noise as shown in Fig. 1.

Our investigation shows that in the few cases where the CAI and IMU phase difference temporarily go beyond the π limit, the difference between the CAI and predicted phase (IMU phase plus the estimated error model) is still below the limit and the filter is able to recover the bias. Therefore, the final estimation of bias and acceleration is not considerably affected by it.

4.2 Hybridization of CAI-ACC with the GRACE-FO E-ACC

For the first test scenario, we consider an electrostatic accelerometer with the same performance as the GRACE-FO accelerometer as discussed in Sect. 2.2. Figure 3 shows the estimated bias as an output of the EKF compared to the true E-ACC bias (non-gravitational signal minus E-ACC measurements). Figure 4 compares the filtered accelerations to the model of non-gravitational accelerations and the measurements of the E-ACC. One can notice the improvements that are achieved in the measured accelerations by using a CAI accelerometer. The Kalman filter also recognises the steep decline in non-gravitational accelerations due to the entry of the satellite into the Earth's penumbra.

To truly compare the output of the filter to the original, one must look at the noise in the frequency domain.

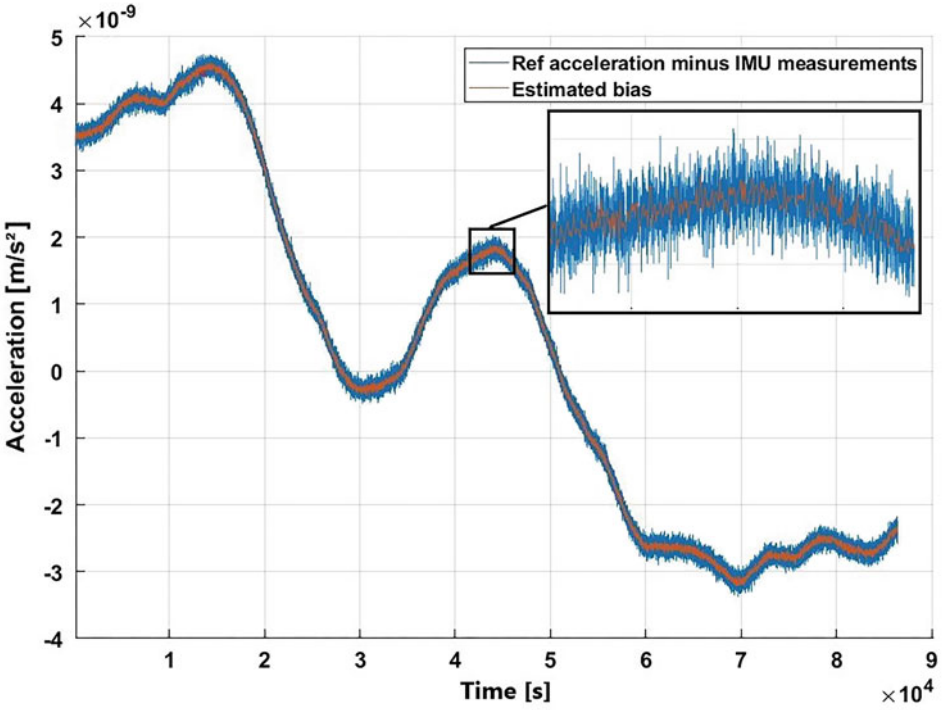

Fig. 3 Blue: The difference between non-gravitational accelerations and the measurements of E-ACC; Magenta: Estimated ACC bias using extended Kalman filtering

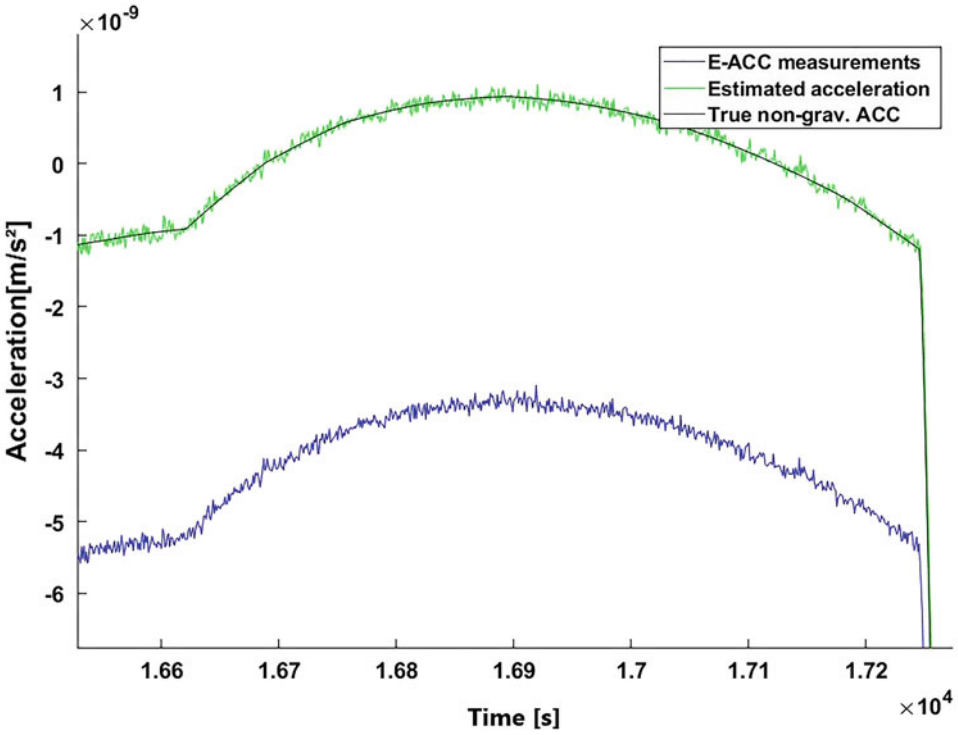

Fig. 4 Short segment of non-gravitational accelerations with measurements of E-ACC (blue), estimated accelerations using the Kalman filter (green) and true non-gravitational accelerations (black) as modelled in XHPS; the steep decline is due to the entry of the satellite into the Earth's penumbra

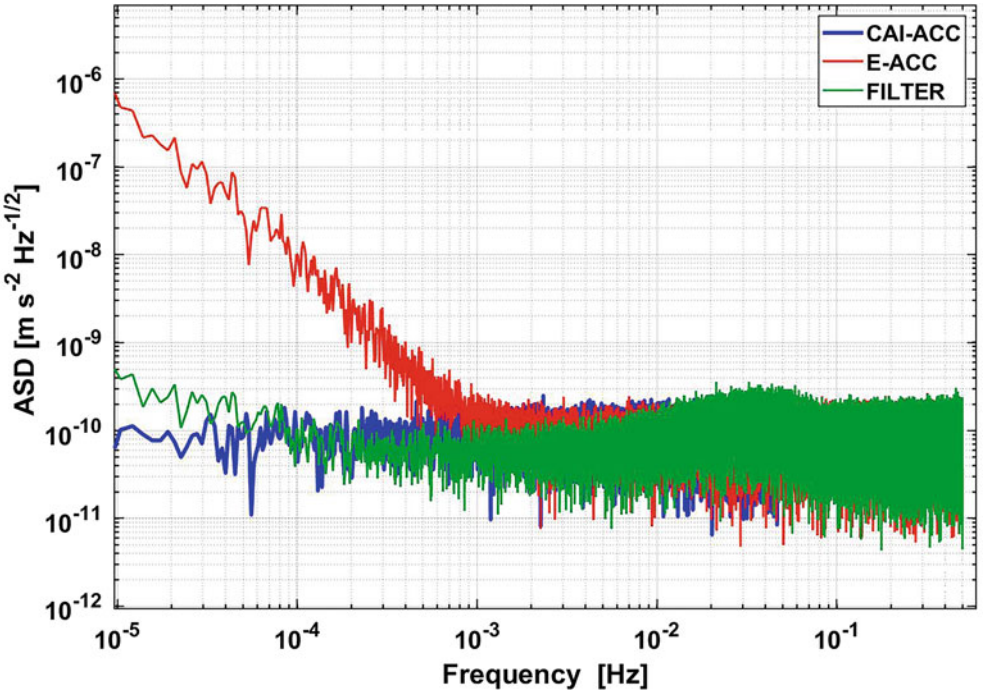

Fig. 5 Hybridization of CAI-ACC with the GRACE-FO E-ACC; spectral representation of the solutions in terms of amplitude spectral density for CAI-ACC (blue) and E-ACC measurements (red), and the Kalman filter (green)

Figure 5 shows the amplitude spectral densities of the CAI and electrostatic accelerometer together with the filter solution, with the modelled non-gravitational accelerations removed. The filter output has gained the accuracy of CAI-ACC measurements at lower frequencies as well as benefiting from the accuracy of E-ACC at higher frequencies.

4.3 Hybridization of CAI-ACC with an Improved E-ACC

In the second test scenario, we assume an E-ACC with a noise level of $10^{-11}\,\mathrm{m/s^2/\sqrt{Hz}}$ in frequencies above 10^{-3} Hz and test the performance of its hybridization with the CAI-ACC model. In this case, because of the higher accuracy of E-ACC, the phase difference between the IMU measurements and the CAI measurements are considerably lower and in most of the cases (>98 %) remain below $\pi/2$ which then leads to a better estimation of the CAI ambiguity.

Figure 6 compares the amplitude spectral densities of the CAI, electrostatic accelerometer together with the filter solution, with the modelled non-gravitational accelerations removed. The filter output has reached the good accuracy of E-ACC measurements at higher frequencies as well as benefiting from the stability of CAI-ACC measurements at lower frequencies. These results, suggest that the described filter is perfectly able to be adopted to different electrostatic and CAI accelerometer accuracies and find the optimal solution in different scenarios.

However, to fully benefit from the instrumental improvements of the quantum accelerometers as well as the LRI, progress to reduce temporal aliasing is also necessary. This is achieved by improved background modelling, e.g., the next generation of AOD products, and deploying multiple satellite pairs. The application of our method in such mission scenarios is part of the ongoing work on this topic.

4.4 Discussion on the Impact of Rotational Accelerations and Gravity Gradient on the Measurements

The effect of rotational accelerations and gravity gradients are not considered in this study. However, here we discuss certain properties which are relevant for CAI measurements. The main rotation, which affects a CAI accelerometer in the along-track direction of a satellite, is the rotation about the cross-track axis due to the orbital frequency. The biggest contribution of this rotation on the atom interferometer phase shift comes from the Coriolis acceleration (Sagnac effect) induced by the atomic velocity in the radial direction (Lévèque et al. 2021).

In addition to the Coriolis acceleration, we have the Euler acceleration and the centrifugal acceleration. However, depending on position and orientation of CAI-ACC in the

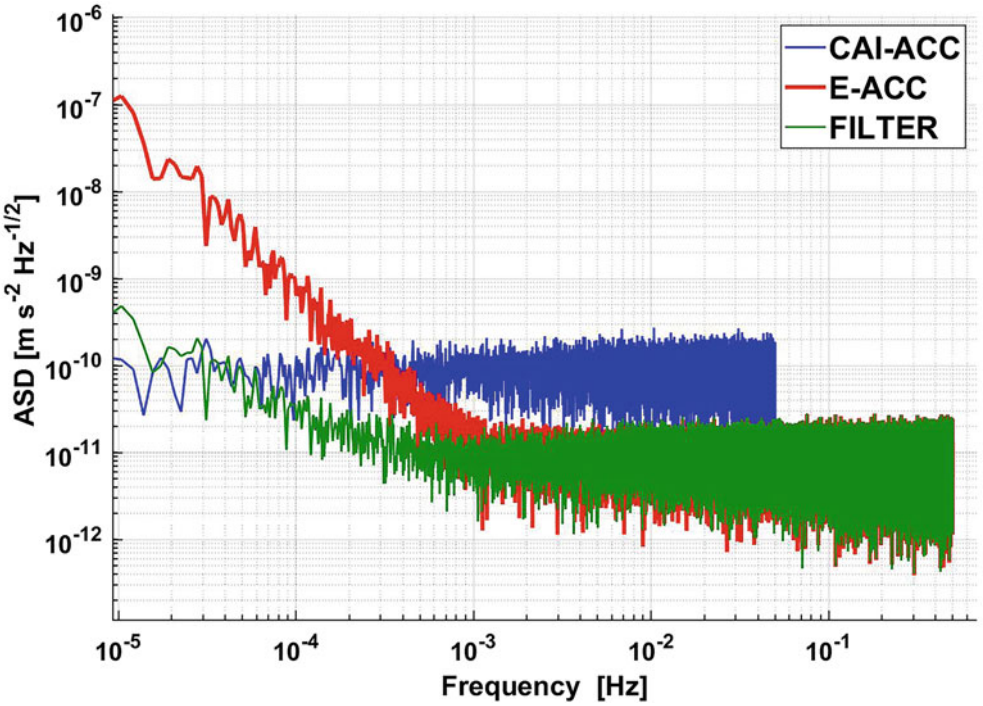

Fig. 6 Hybridization of CAI-ACC with an improved E-ACC; spectral representation of the solutions in terms of amplitude spectral density for CAI-ACC (blue) and E-ACC measurements (red), and the Kalman filter (green)

satellite frame, the CAI-ACC might not see parts of these effects. For example, if the CAI-ACC is placed on top of the E-ACC on the z axis (nadir direction), the centrifugal acceleration would be perpendicular to the CAI-ACC sensitivity axis in along-track direction and therefore, it would not be seen by the instrument. In addition to the rotational accelerations, higher order contributions couple these inertial forces, in particular with gravity gradients. This additional phase shift induces a bias on the measurement of the instrument (Lévèque et al. 2021). The effect of rotational accelerations during one CAI cycle is either physically compensated or the CAI phase shift is calculated and corrected this way. The latter method, however, does not restore the contrast loss due to the Coriolis effect. Therefore, a technical solution would be advantageous.

The impact of the main rotation due to the orbital frequency, can be passively compensated by counter rotating the Raman wave vector, e.g., by designing the laser beam path of the atom interferometer accordingly (see e.g. Migliaccio et al. 2019; Trimeche et al. 2019, for a nadir pointing gradiometer). For the remaining small residual rotation errors, a high performance gyroscope can be used in order to measure the rotation and mathematically cancel its contribution on the output phase shift (Lévèque et al. 2021). The residual rotation errors can also be compensated by active tip-tilt actuation of the retro-reflection mirror (Lan et al. 2012; Migliaccio et al. 2019), preferably mounted directly to the E-ACC housing. Alternatively, the design described by Christophe et al. (2018) for a hybrid accelerometer uses the electrostatic accelerometer proof mass as reference mirror in the Raman interferometer, effectively linking both measurements.

When the E-ACC test mass is in the center of mass of the satellite, the atomic test mass cannot be in the center of mass at the same time. The initial position of the atoms will have an offset with respect to the center of mass after the cooling step of the atom interferometer sequence resulting in a gravity gradient and a gravitational pull of the satellites mass on the atoms. Based on this initial position, which is identical for each atom interferometer sequence, and the mass distribution of the satellite a systematic bias can be calculated and corrected in the atom interferometer phase. The impact of rotational accelerations and positioning of CAI-ACC and E-ACC inside the satellite will be considered in an upcoming study.

Goswami et al. (2021) have shown that the GRACE-FO attitude and orbit control system is capable of controlling the satellites attitude within $\pm 100\,\mu$rad, which is the mission requirement for the pointing accuracy of the LRI (Abich et al. 2019). The beam steering mechanism of the LRI has demonstrated a pointing error below $10\,\mu$rad in the lab (Schütze et al. 2014). Investigations of LRI data estimate the noise of the beam steering to be below $2\,\mu\text{rad}/\sqrt{\text{Hz}}$. The combination of the LRI differential wavefront sensing and beam steering with the star camera and IMU is proposed to increase the overall accuracy of the attitude determination

and therefore, it can be used to further reduce the effect of the satellite rotation on the phase shift (Goswami et al. 2021).

5 Conclusions

Satellite gravity missions successfully map the Earth's gravity field and its change over time. Accelerometers determine the non-gravitational accelerations acting on the satellite. One limiting factor in the gravimetry missions is the accelerometer performance especially in lower frequencies. Using CAI-based accelerometers in the next generation of satellite gravimetry missions can provide long-term stability and precise measurements of the non-gravitational forces acting on the satellites. This would allow a better monitoring of several geophysical phenomena.

We study the hybridization of CAI and electrostatic accelerometers by applying an extended Kalman filter to the measurements. In this approach the classic IMU resolves the high-frequency non-gravitational accelerations while the precision of the calculated hybrid solution benefits from the superior long-term CAI accuracy. Our results show that the EKF can be used to combine the measurements of conventional inertial measurement units with the CAI accelerometers measurements in a way to benefit from both measurements.

For the next generation of satellite gravimetry missions, using a lower altitude and also CAI accelerometers with longer interrogation times will be beneficial. We will study those cases in the future. One major challenge would be that with longer interrogation time, the sensitivity of CAI would be higher and as a result, the dynamical range of the CAI sensor would be smaller. Therefore, one might not be able to determine the CAI ambiguity directly with the measurements of the E-ACC. Drag compensation which would decrease the amplitude of the input accelerations closer to the dynamical range of the CAI-ACC could be a solution here.

In the future, we will also study more complex cases where the impact of rotational rates and gravity gradients are also considered on the CAI measurements and we will compare the achievable accuracy of the recovery of the gravity field with the data from current gravimetry missions. We will also run a number of simulations where we use hybrid accelerometers with different configurations and on different satellite constellations, e.g. on low-altitude drag-free satellites. We will then compare the results to find the optimal scenarios for using hybrid accelerometers in future satellite gravimetry.

Acknowledgements This work is supported by the Deutsche Forschungsgemeinschaft (DFG, German Research Foundation) Collaborative Research Center 1464 "TerraQ" – 434617780 and Germany's Excellence Strategy – EXC-2123 "QuantumFrontiers" – 390837967.

B.T. acknowledges support from the Federal Ministry for Economic Affairs and Energy (BMWi), Project 50RK1957. A.K. acknowledges support from "Niedersächsisches Vorab" through initial funding of research in the DLR-SI institute.

Author Contributions A.H., B.T. designed and performed the main studies. A.H. modelled the electrostatic and CAI accelerometers. B.T. adapted EKF. A.H., B.T., M.S. wrote first draft. A.K. created initial GRACE simulation scenario. All authors provided critical input to the final version.

Data Availability Statement Datasets generated in this study are available from the corresponding author on reasonable request.

References

Abend S, Gersemann M, Schubert C, Schlippert D, Rasel EM, Zimmermann M, Efremov MA, Roura A, Narducci FA, Schleich WP (2020) Atom interferometry and its applications. In: Rasel EM, Schleich W, Wölk S (eds) Proceedings of the international school of physics, vol 197, pp 345–392. https://doi.org/10.3254/978-1-61499-937-9-345

Abich K, Abramovici A, Amparan B, Baatzsch A, Okihiro BB, Barr DC, et al. (2019) In-orbit performance of the GRACE follow-on laser ranging interferometer. Phys Rev Lett 123(3):031101. https://doi.org/10.1103/PhysRevLett.123.031101

Abrykosov P, Pail R, Gruber T, Zahzam N, Bresson A, Hardy E, Christophe B, Bidel Y, Carraz O, Siemes C (2019) Impact of a novel hybrid accelerometer on satellite gravimetry performance. Adv Space Res 63(10):3235–3248. https://doi.org/10.1016/j.asr.2019.01.034

Alonso I, Alpigiani C, Altschul B, Araujo H, Arduini G, Arlt J, Badurina L, Balaz A, Bandarupally S, et al. (2022) Cold atoms in space: Community workshop summary and proposed road-map. https://arxiv.org/abs/2201.07789

Antoine C, Borde CJ (2003) Quantum theory of atomic clocks and gravito-inertial sensors: an update. J Opt B Quantum Semiclass Opt 5(2):S199–S207. https://doi.org/10.1088/1464-4266/5/2/380

Becker D, Lachmann MD, Seidel ST, Ahlers H, Dinkelaker AN, Grosse J, et al. (2018) Space-borne Bose–Einstein condensation for precision interferometry. Nature 562(7727):391–395. https://doi.org/10.1038/s41586-018-0605-1

Christophe B, Boulanger D, Foulon B, Huynh PA, Lebat V, Liorzou F, Perrot E (2015) A new generation of ultra-sensitive electrostatic accelerometers for GRACE Follow-On and towards the next generation gravity missions. Acta Astronaut 117:1–7. https://doi.org/10.1016/j.actaastro.2015.06.021

Christophe B, Foulon B, Liorzou F, Lebat V, Boulanger D, Huynh PA, Zahzam N, Bidel Y, Bresson A (2018) Status of development of the future accelerometers for next generation gravity missions. In: Freymueller JT, Sánchez L (eds) International symposium on advancing geodesy in a changing world, vol 149. Springer International Publishing, Cham, International Association of Geodesy Symposia, pp 85–89. https://doi.org/10.1007/1345_2018_42

Flury J, Bettadpur S, Tapley BD (2008) Precise accelerometry onboard the GRACE gravity field satellite mission. Adv Space Res 42(8):1414–1423. https://doi.org/10.1016/j.asr.2008.05.004

Freier C, Hauth M, Schkolnik V, Leykauf B, Schilling M, Wziontek H, Scherneck HG, Müller J, Peters A (2016) Mobile quantum gravity sensor with unprecedented stability. J Phys Conf Ser 723:012050. https://doi.org/10.1088/1742-6596/723/1/012050

Goswami S, Francis SP, Bandikova T, Spero RE (2021) Analysis of GRACE Follow-On laser ranging interferometer derived intersatellite pointing angles. IEEE Sens J 21(17):19209–19221. https://doi.org/10.1109/JSEN.2021.3090790

Haagmans R, Siemes C, Massotti L, Carraz O, Silvestrin P (2020) ESA's next-generation gravity mission concepts. Rend Lincei-Sci Fis 31:15–25. https://doi.org/10.1007/s12210-020-00875-0

Kasevich M, Chu S (1991) Atomic interferometry using stimulated Raman transitions. Phys Rev Lett 67(2):181–184. https://doi.org/10.1103/PhysRevLett.67.181

Klinger B, Mayer-Gürr T (2016) The role of accelerometer data calibration within GRACE gravity field recovery: Results from ITSG-Grace2016. Adv Space Res 58(9):1597–1609. https://doi.org/10.1016/j.asr.2016.08.007

Knabe A, Schilling M, Wu H, HosseiniArani A, Müller J, Beaufils Q, Pereira dos Santos F (2022) The benefit of accelerometers based on cold atom interferometry for future satellite gravity missions. In: Freymueller J, Sánchez L (eds) Proceedings of the international association of geodesy symposia, Beijing, China, June 28–July 2 2021. https://doi.org/10.1007/1345_2022_151

Lan SY, Kuan PC, Estey B, Haslinger P, Müller H (2012) Influence of the coriolis force in atom interferometry. Phys Rev Lett 108(9):090402. https://doi.org/10.1103/PhysRevLett.108.090402

Loomis BD, Rachlin KE, Wiese DN, Landerer FW, Luthcke SB (2020) Replacing GRACE/GRACE-FO with satellite laser ranging: Impacts on Antarctic ice sheet mass change. Geophys Res Lett 47(3):e2019GL085488. https://doi.org/10.1029/2019GL085488

Lévèque T, Fallet C, Mandea M, Biancale R, Lemoine JM, Tardivel S, Delavault S, Piquereau A, Bourgogne S, Pereira Dos Santos F, Battelier B, Bouyer P (2021) Gravity field mapping using laser coupled quantum accelerometers in space. J Geod 95(15). https://doi.org/10.1007/s00190-020-01462-9

Mandea M, Dehant V, Cazenave A (2020) GRACE—gravity data for understanding the deep Earth's interior. Remote Sens 12(24):4186. https://doi.org/10.3390/rs12244186

Marque JP, Christophe B, Foulon B (2010) Accelerometers of the GOCE mission: return of experience from one year of in-orbit. In: ESA living planet symposium, vol 686, 28.06.–02.07.2010, Bergen, Norway, p 57

Migliaccio F, Reguzzoni M, Batsukh K, Tino GM, Rosi G, Sorrentino F, Braitenberg C, Pivetta T, Barbolla DF, Zoffoli S (2019) MOCASS: A satellite mission concept using cold atom interferometry for measuring the Earth gravity field. Surv Geophys 40(5):1029–1053. https://doi.org/10.1007/s10712-019-09566-4

Pail R, Bingham R, Braitenberg C, Dobslaw H, Eicker A, Güntner A, Horwath M, Ivins E, Longuevergne L, Panet I, Wouters B, IUGG Expert Panel (2015) Science and user needs for observing global mass transport to understand global change and to benefit society. Surv Geophys 36(6):743–772. https://doi.org/10.1007/s10712-015-9348-9

Sanjuan J, Abich K, Blümel L, Gohlke M, Gualani V, Oswald M, Wegehaupt T, Schuldt T, Braxmaier C (2021) Simultaneous laser frequency stabilization to an optical cavity and an iodine frequency reference. Opt Lett 46(2):360–363. https://doi.org/10.1364/OL.413419

Schilling M, Wodey E, Timmen L, Tell D, Zipfel KH, Schlippert D, Schubert C, Rasel EM, Müller J (2020) Gravity field modelling for the Hannover 10 m atom interferometer. J Geod 94(12):122. https://doi.org/10.1007/s00190-020-01451-y

Schütze D, Stede G, Müller V, Gerberding O, Bandikova T, Sheard BS, Heinzel G, Danzmann K (2014) Laser beam steering for GRACE Follow-On intersatellite interferometry. Opt Express 22(20):24117–24132. https://doi.org/10.1364/OE.22.024117

Tapley BD, Watkins MM, Flechtner F, Reigber C, Bettadpur S, Rodell M, et al. (2019) Contributions of GRACE to understanding climate change. Nat Clim Change 9(5):358–369. https://doi.org/10.1038/s41558-019-0456-2

Tennstedt B, Schön S (2021) Integration of atom interferometers and inertial measurement units to improve navigation performance. In: 28th Saint Petersburg International Conference on Integrated Navigation Systems (ICINS), 31.05.–02.06.2021, St. Petersburg, Russia, IEEE, Piscataway, NJ. https://doi.org/10.23919/ICINS43216.2021.9470809

Thomas JB (1999) An analysis of gravity-field estimation based on intersatellite dual-1-way biased ranging. Tech. Rep. JPL Publication 98-15, Jet Propulsion Laboratory, Pasadena, California

Trimeche A, Battelier B, Becker D, Bertoldi A, Bouyer P, Braxmaier C, Charron E, Corgier R, Cornelius M, Douch K, Gaaloul N, Herrmann S, Müller J, Rasel E, Schubert C, Wu H, Pereira Dos Santos F (2019) Concept study and preliminary design of a cold atom interferometer for space gravity gradiometry. Classical Quant Grav 36(21):215004. https://doi.org/10.1088/1361-6382/ab4548

Weddig NB, Tennstedt B, Schön S (2021) Performance evaluation of a three-dimensional cold atom interferometer based inertial navigation system. In: Hecker P (ed) 2021 DGON Inertial Sensors and Systems (ISS), 29.–30.09.2021 IEEE, Braunschweig, Germany, pp 1–20

Wöske F, Kato T, Rievers B, List M (2019) GRACE accelerometer calibration by high precision non-gravitational force modeling. Adv Space Res 63(3):1318–1335. https://doi.org/10.1016/j.asr.2018.10.025